Phase Behavior and Dimensional Scaling of Symmetric Block Copolymer−Homopolymer Ternary Blends in Thin Films

Guoliang Liu, Mark P. Stoykovich, Shengxiang Ji, Karl O. Stuen, Gordon S. W. Craig, and Paul F. Nealey*

Department of Chemical and Biological Engineering, University of Wisconsin−Madison, 1415 Engineering Drive, Madison, Wisconsin 53706

Received December 12, 2008; Revised Manuscript Received February 12, 2009

ABSTRACT: The phase behavior and dimensional scaling of symmetric ternary blends composed of poly(styrene-*block*-methyl methacrylate) block copolymers and the corresponding polystyrene and poly(methyl methacrylate) homopolymers in thin films were investigated as a function of χN (the product of the Flory−Huggins interaction parameter and the overall degree of polymerization of the block copolymer), α (the ratio of the degree of polymerization of the homopolymers to that of the block copolymer), and ϕ_H (the volume fraction of homopolymers in the blends). The phase transitions were characterized by three methods: disappearance of high-order peaks in the fast Fourier transform (FFT) spectra from scanning electron microscopy (SEM) images, application of the amphiphilicity factor determined from the FFTs, and, in the case of thicker films, the appearance of either microphase- or macrophase-separated domains in SEM images. Above the order−disorder transition (ODT) in the $\chi N-\phi_H$ phase diagram, the symmetric ternary blends transitioned from lamellae to a microemulsion and then to macrophase-separated domains as ϕ_H increased. The phase transitions depended weakly on χN and α in the range of $12.7 \le \chi N \le 36.7$ and $0.20 \le \alpha \le 0.99$. The periods of swollen lamellae and microemulsions (L_B) were determined as a function of ϕ_H and α and were well described empirically with $L_B = L_0/(1 - \phi_H)^\beta$, where L_0 is the natural period of pure block copolymer and β is a parameter that depends linearly on α with values ranging from ~0.5 to 1.5.

Introduction

Over the past decades interest has grown in understanding the physics of block copolymer and block copolymer/homopolymer blends in thin (<100 nm) films due to a wide range of potential applications, such as advanced lithography, patterned magnetic media, nanoscale field-effect transistors, spatially limited reactors for the formation of nanoparticles, nanodot arrays, addressable storage media, batteries and fuel cells, and templates for the study of structure−function relationships of biomacromolecules.[1−9] Previous research has demonstrated the use of topographical[7] or chemical[8,9] patterns to direct the assembly of the block copolymer domains and enhance their order, orientation, and registration. The addition of homopolymers to the block copolymer offers a vast array of blend compositions that could provide additional control of dimensional scaling[10,11] and orientation[12] of the block copolymer domains in thin films. Ternary blends, consisting of an A−B block copolymer and the corresponding A and B homopolymers, have drawn significant attention because of their unique and variable phase behavior in the bulk. Because of the ability of the homopolymers to redistribute within the block copolymer morphology, the use of ternary blends facilitates the formation of multiple length scales within a given pattern, which enhances the formation of essential semiconductor pattern geometries such as corners, line terminations, T-junctions, and combinations of lines and spots.[6,13,14] Given their complex phase behavior and potential applications, it is desirable to have a comprehensive understanding of the phase behavior and dimensional scaling of the morphologies of ternary blends in thin films as a function of blend parameters such as the volume fraction of the components, the relative molecular weights of the blend components, and χN, the product of the Flory−Huggins interaction parameter and the degree of polymerization of the block copolymer.

* Corresponding author. E-mail: nealey@engr.wisc.edu.

Much is known from past studies of the phase behavior of ternary mixtures composed of oil, water, and a compatibilizer such as a surfactant.[15−17] In general, the phase diagram of an oil/water/surfactant mixture consists of three distinct regions: a disordered phase, a microemulsion (μE) phase, and a macrophase-separated phase. In ternary polymeric blends, the block copolymer can serve as a compatibilizer for the homopolymers, resulting in phases similar to that of the oil/water/surfactant system, but with the addition of a microphase-separated region to the phase diagram.[18−28] The phase behavior of ternary blends is influenced by many factors, such as the molecular weight and concentration of each component, block copolymer symmetry, temperature, and pressure.[19] Helpful insight can be gained by focusing on symmetric ternary blends, which consist of a symmetric A−B block copolymer, and equal volume fractions of A and B homopolymers ($\phi_A = \phi_B = {}^1/_2\phi_H$) with equal degrees of polymerization ($N_A = N_B = N_H = \alpha N$).[23,25] The use of symmetric ternary blends allows us to examine an isoplethic phase diagram with ϕ_H on the abscissa and χN on the ordinate, as depicted in Scheme 1.

One can examine the phase diagram by considering the case when block copolymer is added to a homopolymer blend ($\phi_H = 1$). In this case, Flory−Huggins (mean-field) theory predicts a second-order phase transition between a disordered and a macrophase separated phase at $\chi N_H = \chi\alpha N = 2$. As block copolymer is added to the homopolymer blend, the order transition line (ODT) between disorder and macrophase separation will follow the Scott line (SL) given by $\chi N_H = 2/\phi_H$.[29] When block copolymer is added to a phase-separated blend of homopolymers, the free energy of the resulting ternary blend is minimized when the block copolymer resides at the A/B interface, with each block protruding into its corresponding homopolymer domain. The reduction in surface tension at the A/B interface and the enthalpic gains of each block residing in the corresponding homopolymer overcome the entropic losses associated with isolating the block copolymer at the domain

10.1021/ma802773h CCC: $40.75
Published on Web 03/26/2009

Scheme 1. Phase Diagram of a Symmetric Ternary Blend[a]

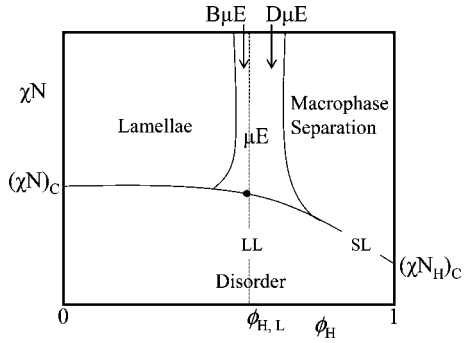

[a] The abscissa is the total volume fraction of homopolymers, ϕ_H; the ordinate is χN. Solid lines are phase transitions. The order−disorder transition (ODT) line starts from the block copolymer critical transition point at $(\chi N)_C = 10.5$ and $\phi_H = 0$ and ends at $(\chi N_H)_C = 2$ and $\phi_H = 1$, as predicted from theory. "SL" denotes the "Scott line". The dashed line labeled "LL" represents the "Lifshitz line". The solid circle on LL is the Lifshitz point (LP). BμE and DμE represent the bicontinuous and droplet regions of the microemulsion channel.

interface and with stretching the block copolymer chains at the interface.[30] As the volume fraction of the block copolymer in the blend is increased, the blend is driven to form new A/B interfaces to place the block copolymer and therefore increasingly smaller phase-separated regions. With the addition of sufficient block copolymer to the blend, the phase-separated regions become small enough that a μE forms. The extent to which new interfaces can be created and populated by block copolymer depends on both N and N_A. Matsen et al. showed with self-consistent-field theory (SCFT) that N cannot be too large because the block copolymer monolayer separating the disparate homopolymer regions must be flexible[31] and that the stiffness of a saturated monolayer of diblock copolymer scales as $\chi^{5/6}N^{4/3}$.[32] In terms of N_A there are competing effects between the configurational entropy loss of homopolymers when they are confined between two block copolymer interfacial monolayers and the translational entropy gained by swelling the copolymer blocks in the interfacial monolayer.[32] The translational entropy is proportional to the number of homopolymer molecules in the system and therefore inversely proportional to N_A. As a result, as N_A increases, the configurational entropy becomes more significant than the translational entropy, eventually leading to the expulsion of homopolymer from between the block copolymer monolayers and the formation of macrophase-separated regions. Thompson et al. showed with SCFT and strong segregation theory (SST) that $\alpha \leq \sim 0.8$ for a μE to occur.[25]

The ternary blend phase diagram can also be examined starting from the $\phi_H = 0$ axis. In this case, for a symmetric block copolymer the ODT will start at $\chi N = 10.5$.[33] As ϕ_H increases, the ODT will be traced out in the phase diagram. Above the ODT, the additional homopolymer will swell the lamellar domains until a transition from lamellar phase to a μE occurs. The transition to the μE phase has been attributed to either fluctuations[19] or phase separation without long-range order.[22] Provided that $\alpha < 1$, the ODT will meet the Scott line at a Lifshitz point (LP),[29] which separates the disordered, macrophase-separated, and microphase-separated regions.[19−21] The coordinates of the Lifshitz points are $\phi_{H,L} = 1/(1 + 2\alpha^2)$ and $\chi N_L = 2/\alpha\phi_{H,L}$.[20] Thus, when $\chi N > \chi N_L$, two transitions exist in the phase diagram above the ODT: the transition between macrophase separation and μE and the transition between the μE and the lamellar region. The space in the phase diagram between these two transitions is known as the microemulsion channel. Depending on the volume fraction of homopolymers, the microemulsion will evolve into either a bicontinuous microemulsion (BμE) at low ϕ_H or a droplet microemulsion (DμE) at high ϕ_H.[26,34−36] The BμE and DμE regions of the phase diagram are separated by the Lifshitz line (LL).

Understanding the ϕ_H location of the micromemulsion channel in the phase diagram is of fundamental and technological importance for the use of ternary blends. A number of ternary blend systems have been investigated experimentally. For example, Bates et al.[37] found the ϕ_H location of the microemulsion channel in the phase diagram of poly(ethylene-*b*-(ethylene-*alt*-propylene)) (P(E-*b*-EP))/polyethylene (PE)/poly(ethylene-*alt*-propylene) (PEP) ternary blends. Similarly, Hillmyer et al. analyzed both P(E-*b*-EP)/PE/PEP ternary blends and poly(ethylene-*b*-ethylene oxide) (P(E-*b*-EO))/PE/poly(ethylene oxide) (PEO) ternary blends and determined the ϕ_H location of the μE channel in their respective phase diagrams.[38] Zhou et al. mapped out the phase diagram and the μE channel in poly(ethylene-*b*-butylene oxide) (P(EP-*b*-BO))/PEP/poly(butylene oxide) (PBO)[39] blends. Corvazier et al. determined both the phase diagram and the distribution of homopolymer in poly(styrene-*b*-isoprene) (P(S-*b*-I))/polystyrene (PS)/polyisoprene (PI) ternary blends.[40] Pipich et al. investigated the phase behavior near the Lifshitz point for poly(styrene-*b*-butadiene) (P(S-*b*-B))/PS/polybutadiene (PB) ternary blends.[34] Morkved et al. also investigated the phase behavior near the Lifshitz point for two sets of ternary blends: poly(ethylethylene-*b*-dimethylsiloxane) (P(EE-*b*-DMS))/polyethylethylene (PEE)/polydimethylsiloxane (PDMS) and poly(ethylene oxide-*b*-ethylenepropylene) (P(EO-*b*-EP))/PEO/PEP.[41] In addition, Bates and co-workers have performed a thorough study of the unusual rheological behavior of ternary blends.[42−45]

Characterization methods that have been used to examine the phase diagrams of ternary blends in the bulk have included small-angle neutron scattering (SANS),[19,39,46,47] small-angle X-ray scattering (SAXS),[39,46,47] transmission electron microscopy (TEM),[19,40,47] optical microscopy,[39] static light scattering,[40] dynamic light scattering,[41,47] rheology,[38,39] cloud point measurements,[38] and visual oil bath measurements.[39] These experiments have focused on the phase diagram as a function of ϕ_H. Although SCFT modeling has predicted that longer homopolymers (larger α) are more efficient at swelling the lamellar domains,[23] and Flory−Huggins lattice theory has suggested that the onset of microemulsion should shift as α varies,[20] we are not aware of any reports of experimentally determined phase diagrams of ternary blends as a function of α.

Although the experimental techniques listed above could be used to determine the phase transitions for blends in the bulk, most are limited for use with thin films due to the experimental setups and the thickness of the films required for measurements. However, the associated experimental data analysis techniques that rely on reciprocal space information can be used with thin films.[48] In the analysis of thin films, it is possible to acquire reciprocal space information, analogous to that obtained from SAXS and SANS, from fast Fourier transforms (FFTs) of the real-space images from scanning electron microscopy (SEM) and TEM, and use that reciprocal space information to determine the phases.[49,50] The use of reciprocal space information from FFTs of thin film images can also allow for the use of scattering models, such as the Teubner−Strey model, which was developed for the analysis of the SANS spectra of small-molecule microemulsions in the bulk.[15−17,48] Since its conception, the Teubner−Strey model has also been applied to microemulsions formed by block copolymer/homopolymer/homopolymer ternary blends.[38,39,47] The use of the Teubner−Strey model in turn offers the possibility to characterize phase transitions with the amphiphilicity factor,[15−17,41] which is a measure of the capability

of the amphiphile, the block copolymer in this work, to compatibilize the homopolymers in the ternary blend.

Related research has focused on the effect of homopolymers on the dimensions of block copolymer domains and the distribution of homopolymers in the blends, which has direct implications in lithographic and template-forming applications. As homopolymers are added to the block copolymer in the bulk, the dimensions of the microphase-separated domains will either swell or shrink into a different period (L_B) than the natural microphase-separated period (L_0) of the block copolymer.[12,23,40,46,51,52] The extent of domain swelling has been described with inverse exponential models as a function of ϕ_H and depends on whether the homopolymer resides in the center of the domain, as is more likely for large α, or is dispersed uniformly throughout the domain, as is more likely for small α.[46,51] Yet we are not aware of any published reports that quantify L_B as a function of both ϕ_H and α.

While the majority of the research on symmetric ternary blends has focused on bulk material, a quantitative and comprehensive knowledge of both the phase behavior and the dimensions of ternary blends in thin films (<100 nm) is needed if one is to direct the self-assembly of a ternary blend into a complicated integrated circuit layout for lithographic applications. Previously, Stoykovich et al. demonstrated the presence of a bicontinuous microemulsion phase in P(S-*b*-MMA)/PS/PMMA ternary blends.[53] Here we employ an array of over 180 different P(S-*b*-MMA)/PS/PMMA blends (all with α < 1) to construct the phase diagrams in both $\chi N-\phi_H$ and $\alpha-\phi_H$ spaces. We demonstrate a new technique that uses the amphiphilicity factor calculated from the Teubner−Strey model to distinguish the weak phase transitions between lamellae, microemulsion, and macrophase separation. Furthermore, we report an empirical dimensional scaling model for L_B as a function of both ϕ_H and α.

Experimental Section

Materials. P(S-*b*-MMA) block copolymers and PS and PMMA homopolymers were purchased from Polymer Source, Inc., and used as received. Hydroxy-terminated poly(styrene-*random*-methyl methacrylate) (58 vol % of styrene) (P(S-*r*-MMA)) was synthesized by "living" free-radical polymerization as described in the literature.[54,55] Five different molecular weights of symmetric P(S-*b*-MMA) were used in the study, with number-average molecular weights (M_n) ranging from 20 to 104 kg/mol. The values of M_n, N, mole fraction of styrene ($f_{styrene}$), χN (χ determined with $\chi = (0.028 \pm 0.002) + (3.9 \pm 0.6)/T$, as reported for P(S-*b*-MMA[56]), and L_0 for the P(S-*b*-MMA) used in the study are listed in Table 1. M_n values of polystyrene (PS) and poly(methyl methacrylate) (PMMA) are listed in Tables 2 and 3. Polished, test grade silicon ⟨100⟩ wafers were purchased from Montco Silicon Technologies, Inc. Toluene (99.8%, anhydrous) was purchased from Sigma-Aldrich, Milwaukee, WI, and was used without further purification.

Sample Preparation. P(S-*r*-MMA) was dissolved in toluene (1.5 wt %) and was spin-coated onto silicon substrates that had been previously cleaned by piranha solution. The initial thicknesses of the polymer films were ∼40 nm. The P(S-*r*-MMA) was grafted onto the silicon substrates by annealing at 160 °C for 48 h under vacuum. The substrates were then rapidly quenched to room temperature after grafting the random copolymers. Ungrafted polymer was removed by repeatedly sonicating the sample in warm toluene. The final polymer film thicknesses were ∼6 nm. Silicon substrates that had been treated with P(S-*r*-MMA) were cleaved into ∼2 cm × 2 cm pieces for further processing.

All of the ternary polymer blends were dissolved in toluene and stirred overnight to form homogeneous solutions with weight concentrations ranging from 0.5% to 1.5%. The compositions of the polymer blends used in this paper are given in terms of volume fractions, and the PS/PMMA homopolymer ratio was fixed at 1:1. Solutions of symmetric ternary blends were spin-coated for 1.5 min onto the P(S-*r*-MMA)-grafted silicon substrates, with spin speeds (4000−6000 rpm) and solution concentrations (0.5−1.5 wt %) selected to yield film thicknesses of approximately L_0. The spin-coated samples were immediately loaded into a vacuum chamber and annealed at 193 °C for 1−15 days. The chamber was purged with argon repeatedly before annealing to minimize the potential degradation by residual oxygen.

Table 1. Characteristics of Pure Block Copolymers

designation	M_n (10^3 g/mol)	N	$f_{styrene}$	χN[a]	L_0[b] (nm)	L_0[c] (nm)
SMMA52−52	104	1020	0.49	36.7	48.4	47.7
SMMA37−37	74	726	0.49	26.1	42.5	45.8
SMMA25−26	51	500	0.48	18.0	33.3	32.8
SMMA18−18	36	353	0.49	12.7	28.5	29.5
SMMA10−10	20	196	0.49	7.1	N/A	N/A

[a] χ is determined according to the literature[56] at the annealing temperature of 190 °C. [b] Determined from samples in thin films with fast Fourier transform (FFT). [c] Determined from samples in the bulk with SAXS.

Table 2. Symmetric Ternary Blends with a Constant α and Various χN

P(S-*b*-MMA) M_n (10^3 g/mol)	PS M_n (10^3 g/mol)	PMMA M_n (10^3 g/mol)	N	N_H	χN	α	$\phi_{H,L}$[a]
52−52	77	75	1020	745	36.7	0.73	0.48
37−37	56.5	52	726	532	26.1	0.73	0.48
25−26	39	37	500	372	18.0	0.74	0.47
18−18	27	25	353	255	12.7	0.72	0.49
10−10	13	15.8	196	141	7.1	0.72	0.49

[a] Calculated according to eq 3.

Table 3. Symmetric Ternary Blends with a Constant χN and Various α

P(S-*b*-MMA) M_n (10^3 g/mol)	PS M_n (10^3 g/mol)	PMMA M_n (10^3 g/mol)	N	N_H	χN	α	$\phi_{H,L}$[a]
52−52	20.8	20	1020	200	36.7	0.20	0.93
52−52	39	37	1020	372	36.7	0.37	0.79
52−52	45	46.5	1020	449	36.7	0.44	0.72
52−52	56.5	52	1020	532	36.7	0.52	0.65
52−52	77	75	1020	745	36.7	0.73	0.48
52−52	102.6	102.7	1020	1007	36.7	0.99	0.34

[a] Calculated according to eq 3.

Instrumentation and Characterization. The film thicknesses were measured with an Auto EL ellipsometer (Rudolph) at three wavelengths (632.8, 546.1, and 405 nm) with an incidence angle of 70° to the sample. The values of the film thicknesses were determined using FilmEllipse software (version 1.1, Scientific Co., Intl.). SEM with an accelerating voltage of 1 kV (LEO 1550 VP FE-SEM) was used to image the annealed samples. In the SEM images, the PS-rich domains appear bright and the PMMA-rich domains appear dark. The bright (and dark) domains obtained in the SEM images were then converted into white (and black) regions with grayscale threshold settings and were further analyzed by FFT to create intensity vs wave vector profiles. SAXS of ∼1 mm thick samples of P(S-*b*-MMA), after 3 days of annealing at 190 °C, were performed on a Rigaku System at Materials Science Center of University of Wisconsin−Madison.

Results and Discussion

Pure Block Copolymer Films on Neutral Substrates. The P(S-*r*-MMA)-grafted silicon substrates exhibited a nonpreferential wetting property for P(S-*b*-MMA), as shown before.[55] On these chemically neutral substrates, the domains of P(S-*b*-MMA) oriented perpendicular to the surface and formed fingerprint-like structures, similar to previous work.[53,55,57−59] Fingerprint structures were observed for the four pure P(S-*b*-MMA) films with the highest M_n, as shown in the top-down SEM images in Figure 1A. The P(S-*b*-MMA) with the lowest M_n exhibited no microphase separation, as expected for a block copolymer with $\chi N = 7.1$.

The two methods used to determine L_0 of the pure P(S-*b*-MMA), SAXS of bulk samples (a 3-D technique) and FFT

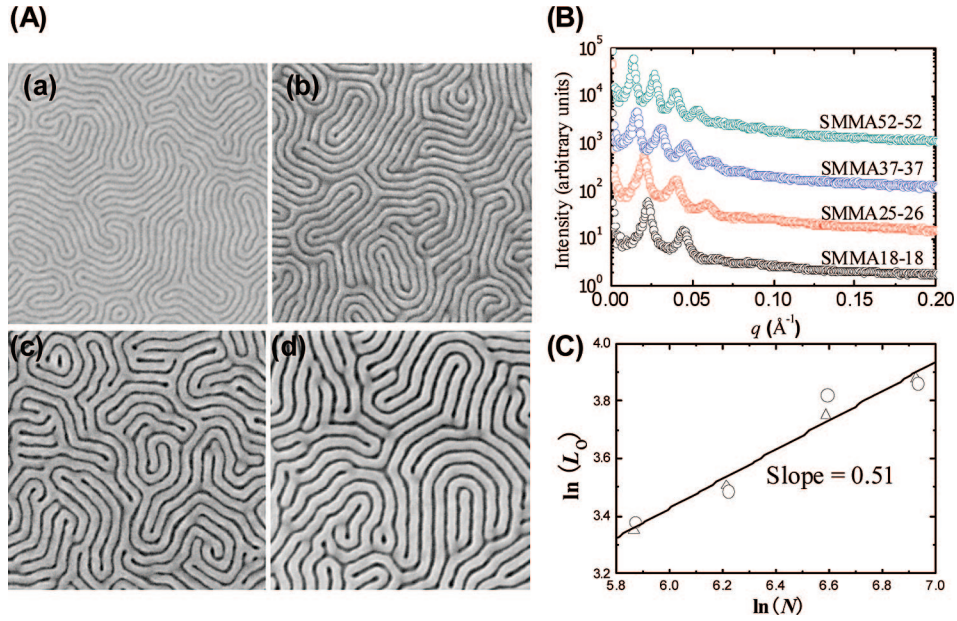

Figure 1. (A) Plan-view SEM images of pure P(S-*b*-MMA) block copolymer thin films, with molecular weights ranging from 36 to 104 kg/mol, on chemically neutral substrates. The film thicknesses are equal to the natural periods of the copolymers. (a) SMMA18−18: $N = 353$; (b) SMMA25−26: $N = 500$; (c) SMMA37−37: $N = 726$; (d) SMMA52−52: $N = 1020$. All micrographs image a 1 μm by 1 μm area. (B) Intensity (I) versus wave vector (q) spectra obtained from FFT analysis of the SEM images in (A). The characteristic (first order) peaks shift toward low q values as the molecular weights of copolymers increase. The units of intensity are arbitrary. (C) L_0 values were calculated according to Bragg's equation, $L_0 = 2\pi/q^*$, and plotted versus N in double-logarithmic coordinates. The slope of the fitted line is 0.51. Upward triangles and circles denote data from FFT analysis and SAXS, respectively.

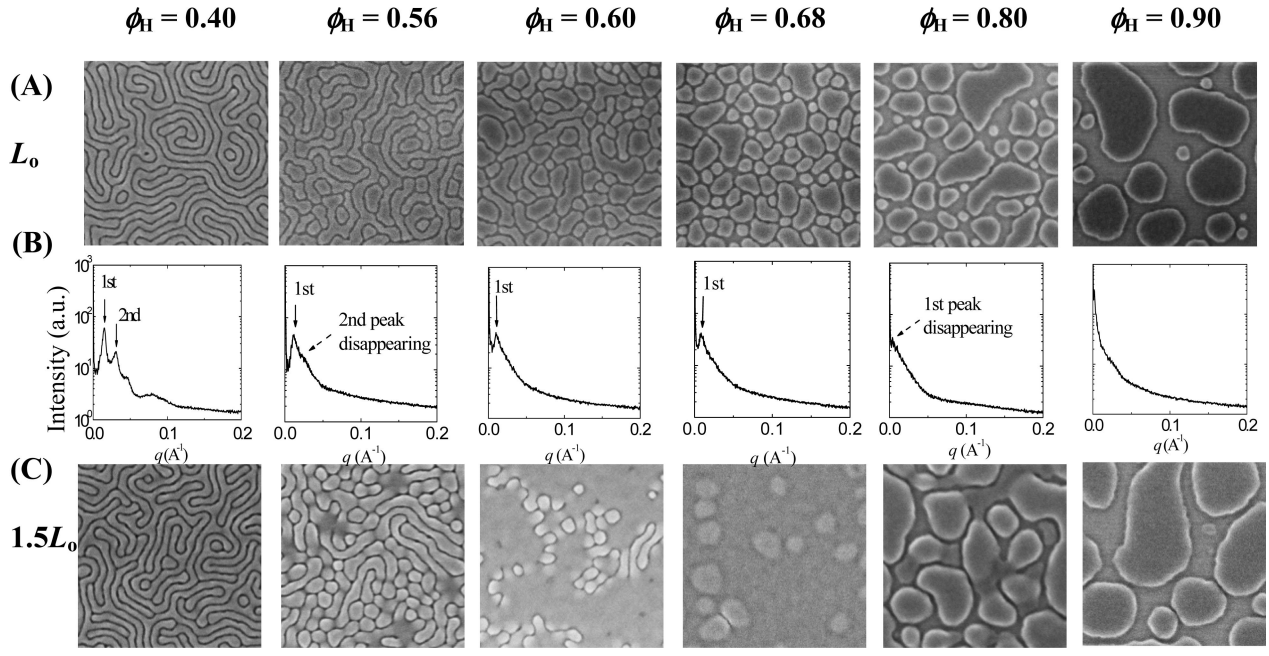

Figure 2. (A) Representative plan-view SEM images and (B) FFT spectra of symmetric ternary blends with $N = 353$, $\alpha = 0.7$, and film thicknesses $= L_0$ on chemically neutral substrates. The volume fractions of homopolymers in the blends (ϕ_H) are denoted above the corresponding images. The disappearance of the second- and first-order peaks from the FFTs indicates the transition points from lamellae to microemulsion and from microemulsion to macrophase separation, respectively. (C) SEM images of the same symmetric ternary blends on chemically neutral substrates with film thicknesses ca. $1.5L_0$. All SEM micrographs image a 1 μm by 1 μm area.

analysis of SEM images of thin film samples (a 2-D technique), gave consistent values of L_0 for all of the microphase-separated samples, as shown in Table 1. FFT analysis of the SEM images in Figure 1A is shown in Figure 1B. In the FFT profiles, the azimuthally averaged Fourier intensity, I, was plotted against the wave vector, q. In the spectra, strong diffraction peaks were present at the positions of $q_n = nq$, where n is an integer, q^* is the characteristic peak, and q_n is the nth-order peak. The higher order diffraction peaks were indicative of lamellar structures,[60] consistent with the real-space SEM images shown in Figure 1A. The positions of the first-order peaks, q^*'s, of the P(S-*b*-MMA) shifted toward smaller q values as N increased. The periods of the copolymers listed in Table 1 were evaluated according to Bragg's equation, $L_0 = 2\pi/q^*$. The fact that FFT, a 2-D characterization technique, and SAXS, a 3-D characterization technique, yielded approximately the same values of L_0 demonstrated that both techniques could be used to characterize the lamellar periods of our P(S-*b*-MMA). The similarity of the

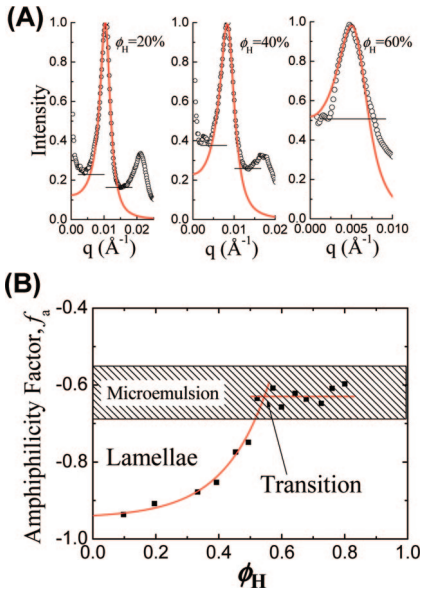

Figure 3. (A) Intensity (I) versus wave vector (q) profiles of symmetric ternary blends ($N = 1020$ and $\alpha = 0.44$) in thin films with representative compositions ($\phi_H = 20\%$, 40%, and 60%). All intensities are normalized. The unit of intensity is arbitrary. The curves are fits to the Teubner−Strey equation. Solid lines define the range of the first-order peaks that were fitted to the model. (B) Amphiphilicity factor, f_a, was calculated according to eq 2 and plotted versus ϕ_H. The shaded area denotes microemulsion. The red lines are exponential and linear fittings to the data from the lamellar and microemulsion phases, respectively. The intercept indicates the transition point from the lamellar phase to the microemulsion phase.

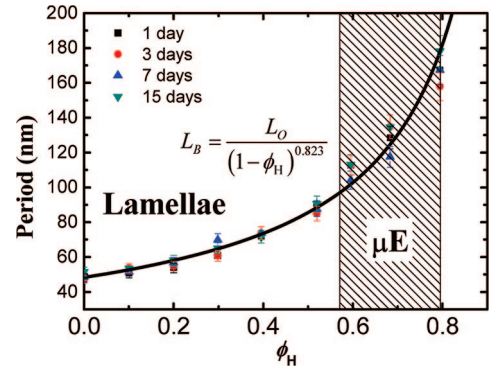

Figure 5. Domain spacings, L_B, of symmetric ternary blends (constant $\chi N = 36.7$ and $\alpha = 0.37$) with lamellae and microemulsion morphologies as a function of homopolymer volume fraction (ϕ_H) for a range of annealing times. The line is a fit to eq 6 with $\beta = 0.81$, demonstrating that the dimensional scaling model can well describe the periods of symmetric ternary blends in the lamellae and microemulsion phases ($R^2 = 0.98$).

results of the 2-D and 3-D characterization techniques was consistent with previous work of directed assembly on chemical patterns, in which the best ordering was achieved when the period of the chemical pattern equaled L_0, suggesting that the morphology of the thin film is thermodynamically driven to assume the same period as in the bulk.[8,9,61,62]

L_0 for the pure P(S-*b*-MMA) scaled as $N^{0.51}$ (fit $R^2 = 0.99$) for N ranging from 353 to 1020 (M_n ranging from 36 to 104 kg/mol), as shown in the plot in Figure 1C. Using a χ value of 0.036 for P(S-*b*-MMA) at the annealing temperature of 190 °C, the corresponding value of χN for this range of M_n ranged from 12.7 to 36.7. The L_0 values and scaling that we found agreed with experimental data for symmetric P(S-*b*-MMA) over the same range of M_n that has been reported by Sivaniah et al. and Green et al.[63,64] Green et al. investigated P(S-*b*-MMA) with M_n values ranging from 84 to 535 kg/mol and determined a scaling law exponent of 0.5. Sivaniah et al. analyzed P(S-*b*-MMA) with N ranging from 274 to 3315. On the basis of the published data of Sivaniah et al. for L_0 in the range of $353 \leq N \leq 1021$, one can calculate a scaling exponent that is much closer to our 0.51 scaling exponent than the 0.85 exponent that Sivaniah et al. experimentally determined for the intermediate segregation regime (ISR).

It is controversial whether P(S-*b*-MMA) in the M_n range used in this study falls in the weak segregation regime (WSR) or the ISR. The $L_0 \propto N^{0.51}$ scaling that we determined is consistent with the $L_0 \propto N^{0.5}$ scaling law initially suggested by Leibler[33] for block copolymers in the WSR. However, since Leibler's seminal work, dimensional scaling laws based on implementations of mean-field theory or self-consistent-field theory have been proposed for the WSR that have exponents ranging from 0.26 to 1.07.[65−70] Additionally, our scaling applies for χN values up to 36.7, whereas previous theoretical work predicts a transition between the WSR and the ISR at $\chi N \sim 13-15$.[68−73] However, Sivaniah et al. experimentally determined that the transition from the WSR to the ISR for P(S-*b*-MMA) was at $\chi N \sim 40$.

Determination of Blend Phases and Transitions. The phase behavior of ternary blends with $N = 353$ and $\alpha = 0.72$, where $\alpha = N_H/N = (N_S N_{MMA})^{1/2}/N$, was analyzed by varying ϕ_H ($\phi_S + \phi_{MMA}$) blended with P(S-*b*-MMA) in 10% increments from

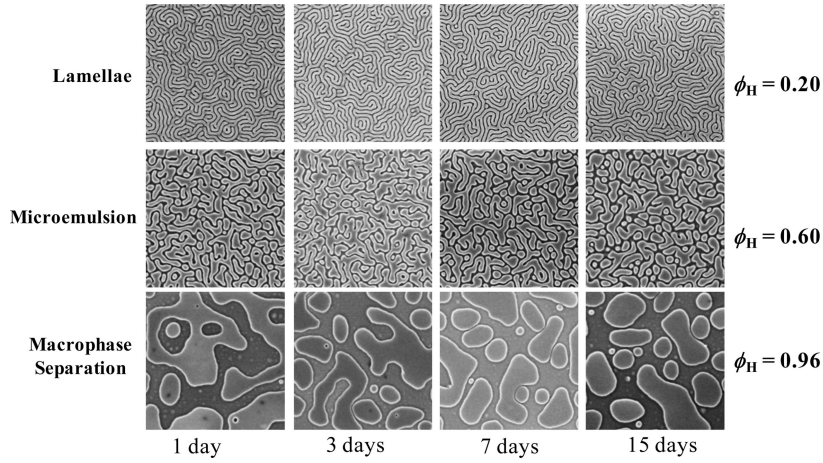

Figure 4. Representative plan-view SEM images of symmetric ternary blends ($N = 1020$ and $\alpha = 0.37$) morphologies as a function of time. All micrographs show a 2 μm by 2 μm area.

0% to 40% and in 4% increment from 40% until macrophase separation occurred. Because FFTs of structures in real space correspond to the scattering patterns in reciprocal space observed in small-angle scattering experiments, we could analyze both real-space data from SEM images and reciprocal-space data from FFT spectra to determine the morphologies formed by symmetric ternary blends. The use of reciprocal-space information from FFT to determine the phase transition points allowed us to obtain data near the forward q region ($q > 0$), which is not easily accessible by conventional X-ray scattering due to the beam stop that blocks small angles. Figure 2A shows a series of SEM images of symmetric ternary blends thin films (each with film thickness $= L_0$) with representative volumetric compositions ($\phi_H = 0.40, 0.56, 0.60, 0.68, 0.80, 0.90$). The high-order peaks in the I vs q graphs obtained from FFTs (Figure 2B) of SEM images of symmetric ternary blends with $\phi_H < 56\%$ demonstrated that the blends possessed a lamellar structure.[51,74] As the amount of homopolymers in the ternary blends was increased to $\phi_H = 56\%$ and larger, the PS domains began to dissociate. At $\phi_H \sim 60\%$, both PS and PMMA domains were still partially continuous, indicative of the BμE phase.[19,75] At $\phi_H \sim 68\%$, all of the PS domains were separated and formed droplets in a matrix of PMMA. As seen in the corresponding FFT analysis (Figure 2B), spectra of both morphologies (BμE and DμE) that formed in the range of $56\% < \phi_H < 80\%$ had only one broad peak in the low q region, indicating that both morphologies were microemulsions.[15−17,74] As ϕ_H was increased further ($\phi_H > 80\%$), the homopolymers macrophase separated into relatively large-scale domains. In the corresponding FFT spectra of the macrophase-separated ternary blends, the first-order peak disappeared and the intensity decreased continuously without a scattering peak present in the low q region.[74] The disappearance of the first-order peak at $\phi_H = 80\%$ and second-order peaks at $\phi_H = 56\%$ can be defined as transition points from microemulsion to macrophase separation and from lamellae to microemulsion, respectively. From the SEM images and FFT analyses, the disappearance of the first and second peak was very gradual with respect to $\Delta\phi_H$. Similar transitions from lamellae to microemulsion and from microemulsion to macrophase separation with increasing amount of homopolymers in the blends were also found in previous studies of ternary blends in the bulk.[37−39]

Another indicator of the phase transitions in thin films of symmetric ternary blends was the strong effect of film thickness on the morphological behavior. Lamellae, microemulsion, and macrophase-separated morphologies could be observed with film thicknesses equal or less than L_0, but the microemulsions behaved differently in thicker films. Representative samples with film thicknesses of $\sim 1.5\ L_0$, shown in Figure 2C, can be compared with the samples with film thicknesses equal to L_0 in Figure 2A. Three characteristics are of particular interest. First, the ternary blends that yielded lamellae ($\phi_H < 56\%$) or macrophase separation ($\phi_H > 80\%$) maintained the same morphologies at the thickness of $1.5L_0$. Second, the ternary blends ($\phi_H = 60\%$ and 68%) that had a microemulsion morphology at a film thickness of L_0 showed only spots or a blanketed morphology at the $1.5L_0$ film thickness, indicating segregation of the homopolymers near the surfaces of the thin films. Third, the symmetric ternary blends with ϕ_H at the transition points (56% or 80%) showed a combination behavior of the two phases they partitioned, validating the transition points determined by FFT analysis. The impact of ϕ_H and film thickness on morphology can be explained phenomenologically by the balance of the thermodynamic factors that drive microphase separation of block copolymers and macrophase separation of incompatible homopolymers as well as the domain orienting effect caused by the neutral surface.[53,76]

The agreement, within experimental error, between the L_0 values determined by SAXS and by FFT (see Figure 1) provided motivation and justification for applying techniques developed for analyzing scattering data of 3-D samples to our 2-D FFT data. Specifically, we used a method based on the determination of the amphiphilicity factor from a fit of the Teubner−Strey model[15] to the FFT spectra to determine phase transitions. The static scattering profile of the microemulsion can be described by the Teubner−Strey equation:

$$I(q) \sim \frac{1}{a_2 + c_1 q^2 + c_2 q^4} \tag{1}$$

where a_2, c_1, and c_2 are associated coefficients that depend on the composition of microemulsion. Typically for microemulsions, $a_2 > 0$, $c_1 < 0$, and $c_2 > 0$, and they fulfill the stability condition $4a_2c_2 - c_1^2 > 0$. The equation could be generalized to other phases such as lamellae and disorder. Schubert et al. determined from the Teubner−Strey equation an amphiphilicity factor, f_a

$$f_a = \frac{c_1}{\sqrt{4a_2c_2}} \tag{2}$$

which is a measurement of the strength of the surfactant in the blends. The amphiphilicity factor of lamellae and disordered structures corresponds to $f_a \sim -1$ and $f_a \sim +1$, respectively.[16,17]

The Teubner−Strey equation (eq 1) was fitted to the FFT spectra of the symmetric ternary blends with $N = 1020$ and $\alpha = 0.44$ to determine a_2, c_1, and c_2. The first peak in the spectra of lamellae (q values between the left and right local minimum of intensity) and microemulsion (q values between the left local minimum of intensity and the point with equal intensity on the right side of the peak) was well characterized by the Teubner−Strey equation, as demonstrated by representative samples with composition of $\phi_H = 20\%$, 40%, and 60% shown in Figure 3A. f_a was calculated according to eq 2 and plotted versus ϕ_H in Figure 3B. As shown in a plot of f_a against ϕ_H, f_a increases monotonically from $f_a \sim -1$ in the lamellar phase, and it levels off to $f_a \sim -0.63$ when the blends reach the microemulsion phase. f_a is fitted exponentially and linearly to ϕ_H in the lamellar and microemulsion phases, respectively. We define the intercept between the two fitted lines as the transition point from lamellae to microemulsion, matching the transition point determined from the disappearance of the second-order peak in the FFT spectra.

To evaluate the stability of the morphologies formed by the symmetric ternary blends, a set of symmetric ternary blend films with thickness $= L_0$, $N = 1020$, and $\alpha = 0.37$ on chemically neutral substrates was annealed for times ranging from 1 to 15 days. Representative samples with lamellae ($\phi_H = 20\%$), microemulsion ($\phi_H = 60\%$), and macrophase separation ($\phi_H = 96\%$) morphologies are shown in Figure 4. The SEM images indicate that both lamellae and microemulsions reached stable morphologies after 1 day, and the size of the microphase-separated domains did not change substantially with continued annealing. A plot of L_B vs ϕ_H (Figure 5) confirmed that the domain period of the lamellar and microemulsion morphologies varied by less than 5% on average with annealing time, indicating that both lamellae and microemulsion were thermodynamically stable morphologies. A simple, one-parameter equation (shown in Figure 5 and described in more detail below) fitted all of the data with an R^2 of 0.98.

$\chi N-\phi_H$ Phase Diagram of Symmetric Ternary Blends in Thin Films. By varying molecular weights of both block copolymers and homopolymers while keeping α constant (0.73 $\pm$ 0.01), we could determine the phase behavior of the ternary

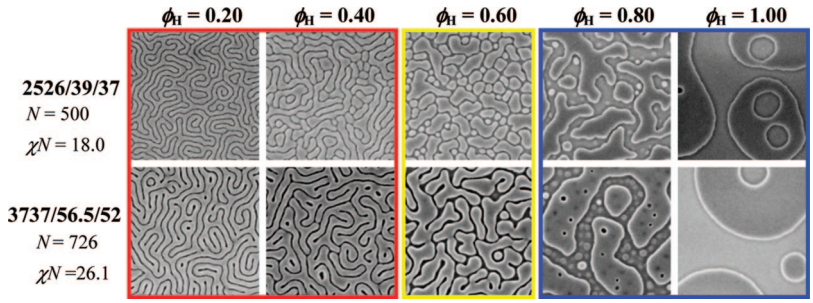

Figure 6. Plan-view SEM images of symmetric ternary blends with constant α = 0.73 and different χN (18.0 and 26.1) on chemically neutral substrates. (Please note that images of χN = 12.7 and 36.7 are shown in Figures 2 and 7, respectively. For χN = 7.1, the blend morphology was disordered and the corresponding images are not shown here.) All film thicknesses were ~L_0 of the P(S-*b*-MMA) copolymer used in the blends. The red, yellow, and blue frames denote lamellae, microemulsion, and macrophase separation, respectively. Only representative compositions of the ternary blends are shown here. Note that samples in the last column with ϕ_H = 1 are binary homopolymer blends. All micrographs image a 1 μm by 1 μm area.

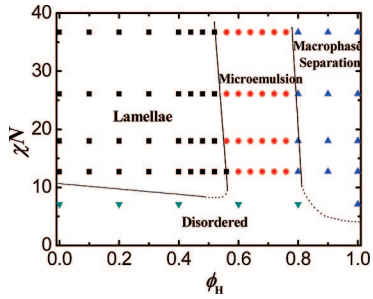

Figure 7. Phase diagram, as determined by SEM and FFT analysis, of symmetric ternary blends as a function of χN and ϕ_H with constant α = 0.73. Black squares, red circles, blue upward triangles, and green downward triangles denote lamellae, microemulsion, macrophase separation, and disordered morphology, respectively. Dashed lines are an estimation of the order−disorder transition (ODT) curve.

blends in thin films as a function of χN and ϕ_H. Assuming χ is independent of composition, χ was determined to be 0.036 at the annealing temperature of 190 °C. With this value of χ applied to a range of N, we could prepare samples that had χN values of 7.1, 12.7, 18.0, 26.1, and 36.7 at the annealing temperature. The investigated symmetric ternary blends systems are summarized in Table 2, and representative SEM images are shown in Figure 6. From the SEM images, symmetric ternary blends with 12.7 ≤ χN ≤ 36.7 formed microphase-separated phases (lamellae and microemulsions) at low ϕ_H and macrophase-separated phases at high ϕ_H. Ternary blends with χN = 7.1 exhibited a disordered morphology at ϕ_H ≤ 80% and macrophase separation at ϕ_H = 100%. On the basis of the FFT analysis of the SEM images and the f_a values calculated for these samples, a phase diagram for the symmetric ternary blends with constant α was constructed, as shown in Figure 7. The solid lines denote the transition from lamellae to microemulsion and the transition from microemulsion to macrophase separation. The dashed lines are an estimate of the order−disorder transition (ODT).

In the χN−ϕ_H phase diagram (Figure 7), the location of the microemulsion channel did not shift significantly despite χN changing from 12.7 to 36.7, indicating the phase transitions are weakly dependent on χN for P(S-*b*-MMA)/PS/PMMA symmetric ternary blends in thin films. Although we have drawn the phase diagram in the range of χN ≤ 36.7, we cannot rule out the possibility of the existence of other morphologies at larger χN for P(S-*b*-MMA)/PS/PMMA symmetric ternary blends.

α−ϕ_H Phase Diagram and Dimensional Scaling of Symmetric Ternary Blends in Thin Films. The effect of the homopolymer chain length was studied in more detail by varying α while maintaining a constant χN (=36.7). According to the theoretical predictions, the microemulsion channel should shift to a lower ϕ_H as α increases, as shown by[20]

$$\phi_{H,L} = \frac{1}{1 + 2\alpha^2} \tag{3}$$

In this study, we systematically varied α from 0.20 to 0.99. The ternary blends systems that we investigated are summarized in Table 3, and representative SEM images of blends with α = 0.20, 0.37, 0.44, 0.52, 0.73, and 0.99 are shown in Figure 8. The resulting α−ϕ_H phase diagram of symmetric ternary blends with a constant χN is shown in Figure 9. The trend of the microemulsion channel shifting toward a lower ϕ_H can be clearly observed in the phase diagram. In contrast to the theoretical prediction of the onset of microemulsion of ternary blends in the bulk at the $\phi_{H,L}$[20] (eq 3), the onset of the microemulsion phase from the experimental data presented here shows a much slower shifting trend in the range of 0.20 ≤ α ≤ 0.99 for P(S-*b*-MMA)/PS/PMMA ternary blends in thin films. Particularly, lamellar morphologies could be observed at ϕ_H = 10% for α up to 4.52, which theory[20] predicts not to be in the lamellar phase.

As shown in Figure 8, the domain spacing of the symmetric ternary blends increased as ϕ_H increased. In blends with a larger α, it increased more than those with a smaller α at the same ϕ_H. Previously, Torikai et al.[51] put forward a model describing the extent that homopolymers swell the domains of the block copolymer in the bulk. Two ideal cases were presented: if all homopolymers are distributed uniformly in the corresponding domain, the lamellae will be swollen as

$$L_B = \frac{L_0}{(1 - \phi_H)^{1/3}} \tag{4}$$

whereas if the homopolymers are localized perfectly at the center of the domain or packed freely inside the block copolymer chains, the lamellae will be swollen as

$$L_B = \frac{L_0}{1 - \phi_H} \tag{5}$$

We determined that the dependence of L_B on ϕ_H and α, over the range of M_n and ϕ_H values examined in this study, could be quantified by a simple, empirical relationship:

$$L_B = \frac{L_0}{(1 - \phi_H)^{\beta}} \tag{6}$$

where L_0 is the period of pure block copolymer depending on the molecular weight of block copolymer and β is a function of α.

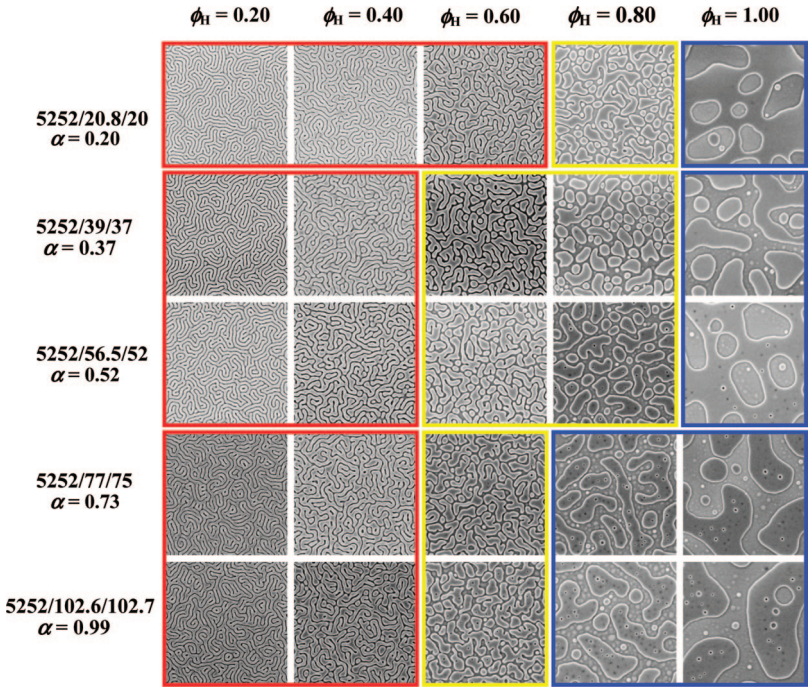

Figure 8. Plan-view SEM images of symmetric ternary blends with constant $\chi N = 36.7$ and a range of α values on chemically neutral substrates. All film thicknesses were $\sim L_0$ of the P(S-*b*-MMA). The red, yellow, and blue frames denote lamellae, microemulsion, and macrophase separation, respectively. Only representative compositions of the ternary blends are shown here. Note that samples in the last column with $\phi_H = 1$ are binary homopolymer blends. All micrographs image a 2 μm by 2 μm area.

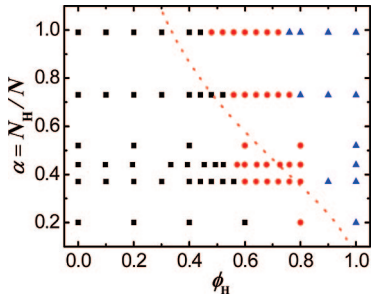

Figure 9. Phase diagram of symmetric ternary blends as a function of α and ϕ_H with constant $\chi N = 36.7$. Black squares, red circles, and blue triangles denote lamellae, microemulsion, and macrophase separation, respectively. The dashed line is the theoretical prediction of the Lifshitz line.

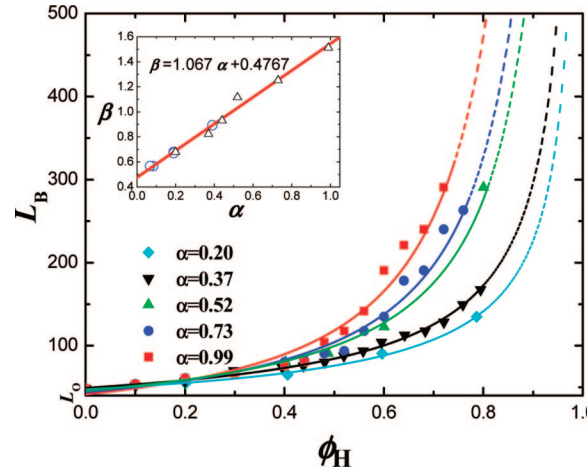

Figure 10. Domain spacings, L_B, of symmetric ternary blends (constant $\chi N = 36.7$ and various $\alpha = 0.2-0.99$), with lamellae and microemulsion morphologies, as a function of ϕ_H. L_0 denotes the natural period of SMMA52−52 copolymer. The solid lines are least-squares fits of eq 6 to the data, and the dashed lines are extrapolations to larger ϕ_H. The dependence of β on α is shown in the inset. Triangles denote our β values, and the circles denote β values determined from eq 6 for P(S-*b*-I)/PS/PI and P(S-*b*-2VP)/PS/P2VP blends from the literature.

The periods, L_B, of microphase-separated lamellae and microemulsion blends with $N = 1020$ and various α were evaluated according to the Bragg's equation, $L_B = 2\pi/q^*$, and plotted against ϕ_H in Figure 10. As discussed above in Figure 5, the periods of microphase-separated symmetric ternary blends with $N = 1020$ ($L_0 = 48.4$ nm) and $\alpha = 0.37$ did not change significantly as a function of time, and all of the data in Figure 5 could be fit by eq 6 with $\beta = 0.82$ (fit $R^2 = 0.98$). The five curves shown in Figure 10 are least-squares fits of the data to eq 6. The fit to each set of data had its unique β value, and the fitted curves all overlapped at $\phi_H = 0$ with $L_B = L_0 = 48.4$ nm. The fitted curves demonstrate that eq 6 could well describe the domain spacing of the symmetric ternary blends in thin films.

The fitted β value for blends system with different α were plotted against α in the inset of Figure 10. From the obtained data, β increased monotonically with increasing α, implying that longer homopolymers are more efficient at swelling the lamellar domains, as has been predicted by modeling with self-consistent-field theory.[23] A linear dependence of β on α was found to be

$$\beta = 1.07\alpha + 0.477 \quad (7)$$

For comparison, we also plotted β as a function of α in the inset of Figure 10 for P(S-*b*-I)/PS/PI blends[40,52] and poly(styrene-*b*-2-vinylpyridine) P(S-*b*-2VP)/PS/poly(2-vinylpyridine) (P2VP) blends[51] in the bulk reported in the literature.

Three characteristics are of interest in Figure 10 and the fitted functions. First, for symmetric ternary blends with $\alpha = 0.5$, L_B can be estimated by eq 6 with $\beta = 1.01$. This corresponds to Torikai's model shown in eq 5, indicating that homopolymers

with chain lengths equal to their corresponding blocks of the block copolymer can be packed freely inside the block copolymer domains.[51] The second characteristic of note relates to the swelling behavior of homopolymers with infinitely small chain length (i.e., $\alpha = 0$). For such a hypothetical blend, the predicted value by Torikai et al. is $\beta = 1/3$, with an assumption that all the homopolymers are distributed uniformly in the corresponding domains of the block copolymer.[51] If we extrapolate eq 7 to $\alpha = 0$, L_B can be estimated by eq 6 with $\beta = 0.477$. This discrepancy may indicate that the homopolymers are actually distributed nonuniformly in the blends, which has been previously observed,[40] resulting in the swelling of block domains more than in the ideal case. Third, the model used in this work (eq 6) can be extended to estimate L_B for other symmetric ternary blends such as P(S-*b*-I)/PS/PI and P(S-*b*-2VP)/PS/P2VP, and it can be generalized to symmetric ternary blends in the bulk. For example, by fitting eq 6 to the data of P(S-*b*-I)/PS/PI ternary blends in the bulk with $\alpha = 0.068$ and 0.190 from Tanaka[52] and Corvazier's work,[40] $\beta = 0.567$ and 0.670, respectively, which matches well with β estimates of 0.549 (<4% difference) and 0.679 (<2% difference) from eq 7. This validates that the dimensional scaling model shown in eqs 6 and 7 can be used to estimate the swollen behavior of block copolymers by homopolymers in symmetric ternary blends, both in thin films and in the bulk.

Conclusion

This work provides the first detailed quantification of the phase diagram of symmetric ternary blends in thin films. We developed and validated an FFT method for determining the phase boundaries of symmetric ternary blends in thin films. We also demonstrated the use of the amphiphilicity factor to determine the location of the transition from the microphase separated to the microemulsion morphology. The periods of the swollen lamellae and microemulsions (L_B) can be empirically scaled with a simple model, which offers insight into the distribution of homopolymers within the domains of the blend. The methodology presented here is sufficiently generalized such that the determination of the phase diagrams or the amount of domain swelling in other symmetric ternary blends should be possible. Our methodology should also assist in the determination of phase transitions and the development of dimensional scaling models for asymmetric block copolymer blends, including blends with asymmetric block copolymers or blends with asymmetric compositions of the components, and block copolymer blends with composites and nanoparticles. Such knowledge in turn could assist in the development of ternary blend systems that could be used in thin film applications such as advanced lithography, in which multiple length scales are necessary for patterns with a variety of semiconductor fabric architectures.

Acknowledgment. This work was supported by the Semiconductor Research Corporation (SRC) and NSF through the UW-Nanoscale Science and Engineering Center (NSEC) (Grant DMR0425880).

References and Notes

(1) Cheng, J. Y.; Ross, C. A.; Smith, H. I.; Thomas, E. L. *Adv. Mater.* **2006**, *18*, 2505.
(2) Hawker, C. J.; Russell, T. P. *MRS Bull.* **2005**, *30*, 952.
(3) Nealey, P. F.; Edwards, E. W.; Müller, M.; Stoykovich, M. P.; Solak, H. H.; De Pablo, J. J. *IEEE Tech. Dig. IEDM* **2005**, 356.
(4) Park, M.; Harrison, C.; Chaikin, P. M.; Register, R. A.; Adamson, D. H. *Science* **1997**, *276*, 1401.
(5) Segalman, R. A. *Mater. Sci. Eng., R* **2005**, *48*, 191.
(6) Stoykovich, M. P.; Nealey, P. F. *Mater. Today* **2006**, *9*, 20.
(7) Segalman, R. A.; Yokoyama, H.; Kramer, E. J. *Adv. Mater.* **2001**, *13*, 1152.
(8) Kim, S. O.; Solak, H. H.; Stoykovich, M. P.; Ferrier, N. J.; de Pablo, J. J.; Nealey, P. F. *Nature (London)* **2003**, *424*, 411.
(9) Rockford, L.; Liu, Y.; Mansky, P.; Russell, T. P.; Yoon, M.; Mochrie, S. G. J. *Phys. Rev. Lett.* **1999**, *82*, 2602.
(10) Edwards, E. W.; Stoykovich, M. P.; Nealey, P. F.; Solak, H. H. *J. Vac. Sci. Technol., B* **2006**, *24*, 340.
(11) Jeong, U.; Ryu, D. Y.; Kho, D. H.; Lee, D. H.; Kim, J. K.; Russell, T. P. *Macromolecules* **2003**, *36*, 3626.
(12) Kitano, H.; Akasaka, S.; Inoue, T.; Chen, F.; Takenaka, M.; Hasegawa, H.; Yoshida, H.; Nagano, H. *Langmuir* **2007**, *23*, 6404.
(13) Stoykovich, M. P.; Muller, M.; Kim, S. O.; Solak, H. H.; Edwards, E. W.; de Pablo, J. J.; Nealey, P. F. *Science* **2005**, *308*, 1442.
(14) Kang, H.; Craig, G. S. W.; Nealey, P. *J. Vac. Sci. Technol.* **2008**, *26*, 2495.
(15) Teubner, M.; Strey, R. *J. Chem. Phys.* **1987**, *87*, 3195.
(16) Schubert, K. V.; Strey, R. *J. Chem. Phys.* **1991**, *95*, 8532.
(17) Schubert, K. V.; Strey, R.; Kline, S. R.; Kaler, E. W. *J. Chem. Phys.* **1994**, *101*, 5343.
(18) Muller, M.; Schick, M. *J. Chem. Phys.* **1996**, *105*, 8885.
(19) Bates, F. S.; Maurer, W. W.; Lipic, P. M.; Hillmyer, M. A.; Almdal, K.; Mortensen, K.; Fredrickson, G. H.; Lodge, T. P. *Phys. Rev. Lett.* **1997**, *79*, 849.
(20) Broseta, D.; Fredrickson, G. H. *J. Chem. Phys.* **1990**, *93*, 2927.
(21) Hornreich, R. M.; Luban, M.; Shtrikman, S. *Phys. Lett. A* **1975**, *55*, 269.
(22) Komura, S. *J. Phys.: Condens. Matter* **2007**, *19*, 463101.
(23) Komura, S.; Kodama, H.; Tamura, K. *J. Chem. Phys.* **2002**, *117*, 9903.
(24) Naughton, J. R.; Matsen, M. W. *Macromolecules* **2002**, *35*, 8926.
(25) Thompson, R. B.; Matsen, M. W. *J. Chem. Phys.* **2000**, *112*, 6863.
(26) Duchs, D.; Schmid, F. *J. Chem. Phys.* **2004**, *121*, 2798.
(27) Duchs, D.; Ganesan, V.; Fredrickson, G. H.; Schmid, F. *Macromolecules* **2003**, *36*, 9237.
(28) Janert, P. K.; Schick, M. *Macromolecules* **1997**, *30*, 3916.
(29) Fredrickson, G. H.; Bates, F. S. *J. Polym. Sci., Part B: Polym. Phys.* **1997**, *35*, 2775.
(30) Noolandi, J.; Hong, K. M. *Macromolecules* **1982**, *15*, 482.
(31) Matsen, M. W. *J. Chem. Phys.* **1999**, *110*, 4658.
(32) Thompson, R. B.; Matsen, M. W. *Phys. Rev. Lett.* **2000**, *85*, 670.
(33) Leibler, L. *Macromolecules* **1980**, *13*, 1602.
(34) Pipich, V.; Schwahn, D.; Willner, L. *Appl. Phys. A: Mater. Sci. Process.* **2002**, *74*, S345.
(35) Pipich, V.; Schwahn, D.; Willner, L. *J. Chem. Phys.* **2005**, 123.
(36) Pipich, V.; Schwahn, D.; Willner, L. *Phys. Rev. Lett.* **2005**, 94.
(37) Koneripalli, N.; Singh, N.; Levicky, R.; Bates, F. S.; Gallagher, P. D.; Satija, S. K. *Macromolecules* **1995**, *28*, 2897.
(38) Hillmyer, M. A.; Maurer, W. W.; Lodge, T. P.; Bates, F. S.; Almdal, K. *J. Phys. Chem. B* **1999**, *103*, 4814.
(39) Zhou, N.; Lodge, T. P.; Bates, F. S. *J. Phys. Chem. B* **2006**, *110*, 3979.
(40) Corvazier, L.; Messe, L.; Salou, C. L. O.; Young, R. N.; Fairclough, J. P. A.; Ryan, A. J. *J. Mater. Chem.* **2001**, *11*, 2864.
(41) Morkved, T. L.; Stepanek, P.; Krishnan, K.; Bates, F. S.; Lodge, T. P. *J. Chem. Phys.* **2001**, *114*, 7247.
(42) Zhou, N.; Bates, F. S.; Lodge, T. P.; Burghardt, W. R. *J. Rheol.* **2007**, *51*, 1027.
(43) Krishnan, K.; Bates, F. S.; Lodge, T. P. *J. Rheol.* **2005**, *49*, 1395.
(44) Krishnan, K.; Burghardt, W. R.; Lodge, T. P.; Bates, F. S. *Langmuir* **2002**, *18*, 9676.
(45) Krishnan, K.; Chapman, B.; Bates, F. S.; Lodge, T. P.; Almdal, K.; Burghardt, W. R. *J. Rheol.* **2002**, *46*, 529.
(46) Matsushita, Y.; Torikai, N.; Mogi, Y.; Noda, I.; Han, C. C. *Macromolecules* **1993**, *26*, 6346.
(47) Morkved, T. L.; Chapman, B. R.; Bates, F. S.; Lodge, T. P.; Stepanek, P.; Almdal, K. *Faraday Discuss.* **1999**, 335.
(48) Stoykovich, M. P.; Edwards, E. W.; Solak, H. H.; Nealey, P. F. *Phys. Rev. Lett.* **2006**, *97*, 147802.
(49) Kane, L.; Satkowski, M. M.; Smith, S. D.; Spontak, R. J. *Macromolecules* **1996**, *29*, 8862.
(50) Park, S. Y.; Chang, Y. J.; Farmer, B. L. *Langmuir* **2006**, *22*, 11369.
(51) Torikai, N.; Takabayashi, N.; Noda, I.; Koizumi, S.; Morii, Y.; Matsushita, Y. *Macromolecules* **1997**, *30*, 5698.
(52) Tanaka, H.; Hasegawa, H.; Hashimoto, T. *Macromolecules* **1991**, *24*, 240.
(53) Stoykovich, M. P.; Edwards, E. W.; Solak, H. H.; Nealey, P. F. *Phys. Rev. Lett.* **2006**, *97*, 147802.
(54) Husseman, M.; Malmstrom, E. E.; McNamara, M.; Mate, M.; Mecerreyes, D.; Benoit, D. G.; Hedrick, J. L.; Mansky, P.; Huang, E.; Russell, T. P.; Hawker, C. J. *Macromolecules* **1999**, *32*, 1424.
(55) Mansky, P.; Liu, Y.; Huang, E.; Russell, T. P.; Hawker, C. *Science* **1997**, *275*, 1458.

(56) Russell, T. P.; Hjelm, R. P.; Seeger, P. A. *Macromolecules* **1990**, *23*, 890.
(57) Ryu, D. Y.; Shin, K.; Drockenmuller, E.; Hawker, C. J.; Russell, T. P. *Science* **2005**, *308*, 236.
(58) Ji, S. X.; Liu, G. L.; Zheng, F.; Craig, G. S. W.; Himpsel, F. J.; Nealey, P. F. *Adv. Mater.* **2008**, *20*, 3054.
(59) In, I.; La, Y. H.; Park, S. M.; Nealey, P. F.; Gopalan, P. *Langmuir* **2006**, *22*, 7855.
(60) Sakurai, S.; Momii, T.; Taie, K.; Shibayama, M.; Nomura, S.; Hashimoto, T. *Macromolecules* **1993**, *26*, 485.
(61) Edwards, E. W.; Montague, M. F.; Solak, H. H.; Hawker, C. J.; Nealey, P. F. *Adv. Mater.* **2004**, *16*, 1315.
(62) Ruiz, R.; Sandstrom, R. L.; Black, C. T. *Adv. Mater.* **2007**, *19*, 587.
(63) Green, P. F.; Russell, T. P.; Jerome, R.; Granville, M. *Macromolecules* **1988**, *21*, 3266.
(64) Sivaniah, E.; Matsubara, S.; Zhao, Y.; Hashimoto, T.; Fukunaga, K.; Kramer, E. J.; Mates, T. E. *Macromolecules* **2008**, *41*, 2584.
(65) De La Cruz, M. O. *Phys. Rev. Lett.* **1991**, *67*, 85.
(66) Rebei, A.; De Pablo, J. *Phys. Rev. E* **2001**, 6304.
(67) Shull, K. R. *Macromolecules* **1992**, *25*, 2122.
(68) Sones, R. A.; Terentjev, E. M.; Petschek, R. G. *Macromolecules* **1993**, *26*, 3344.
(69) Whitmore, M. D.; Noolandi, J. *J. Chem. Phys.* **1990**, *93*, 2946.
(70) Matsen, M. W.; Bates, F. S. *Macromolecules* **1996**, *29*, 1091.
(71) Melenkevitz, J.; Muthukumar, M. *Macromolecules* **1991**, *24*, 4199.
(72) Matsen, M. W.; Bates, F. S. *J. Chem. Phys.* **1997**, *106*, 2436.
(73) Lescanec, R. L.; Muthukumar, M. *Macromolecules* **1993**, *26*, 3908.
(74) Hamley, I. W. *The Physics of Block Copolymers*; Oxford University Press: New York, 1998.
(75) Jinnai, H.; Hasegawa, H.; Nishikawa, Y.; Sevink, G. J. A.; Braunfeld, M. B.; Agard, D. A.; Spontak, R. J. *Macromol. Rapid Commun.* **2006**, *27*, 1424.
(76) Huang, E.; Rockford, L.; Russell, T. P.; Hawker, C. J. *Nature (London)* **1998**, *395*, 757.

MA802773H